Nano Energy 76 (2020) 105046

Contents lists available at ScienceDirect

Nano Energy

journal homepage: http://www.elsevier.com/locate/nanoen

Grafting polymer from oxygen-vacancy-rich nanoparticles to enable protective layers for stable lithium metal anode

Sipei Li [a,1], Tong Liu [a,1], Jiajun Yan [a,1], Jacob Flum [a], Han Wang [b], Francesca Lorandi [a], Zongyu Wang [a], Liye Fu [a], Leiming Hu [c], Yuqi Zhao [b], Rui Yuan [a], Mingkang Sun [a], Jay F. Whitacre [b,d,*], Krzysztof Matyjaszewski [a,**]

[a] Department of Chemistry, Carnegie Mellon University, 4400 Fifth Ave, Pittsburgh, PA, 15213, USA
[b] Department of Materials Science and Engineering, Carnegie Mellon University, 5000 Forbes Ave, Pittsburgh, PA, 15213, USA
[c] Department of Mechanical Engineering, Carnegie Mellon University, 5000 Forbes Ave, Pittsburgh, PA, 15213, USA
[d] Scott Institute for Energy Innovation, Carnegie Mellon University, 5000 Forbes Ave, Pittsburgh, PA, 15213, USA

ARTICLE INFO

Keywords:
Artificial SEI
Lithium metal battery
YSZ
SI-ATRP
Polymer hybrids
Lithium dendrite

ABSTRACT

Fabricating an artificial solid electrolyte interface (SEI) is a promising approach to improve cycling stability of lithium metal batteries. In this work, a new category of artificial SEI based on oxygen vacancy-rich hybrid nanoparticles was prepared by covalently grafting polymers from yttria–stabilized zirconia (YSZ) nanoparticles via surface-initiated atom transfer radical polymerization (SI-ATRP). The hairy nanoparticles had high dispersibility in dimethylsulfoxide, and were solution casted into uniform thin films with high inorganic content, high ionic conductivity ($>1 \times 10^{-4}$ S/cm at r.t.), and good mechanical properties (Young's modulus 7.56 GPa). No dendrite formation was observed by *in-situ* optical microscopy on a lithium metal protected by such artificial SEI. Protected anodes were stably cycled at 3 mA/cm^2 and 3 mA h/cm^2 with low overpotentials (20 mV) for >2500 h. $LiNi_{0.8}Co_{0.15}Al_{0.05}O_2$ (NCA)|Li full cells with protected Li anode showed much higher specific discharge capacity at various rates and improved capacity retention compared to unprotected Li anode.

1. Introduction

Despite the huge market success of lithium ion batteries (LIB), the research community continues to seek a battery technology that is "beyond LIB" with higher energy densities and at least comparable cycling stability [1,2]. Encouraging advancements have been made in anode, cathode and electrolyte components [3–10]. Yet the fundamental part of this quest is widely recognized as enabling the use of lithium metal anode, which has the lowest redox potential (−3.040 V vs. the standard hydrogen electrode) and highest theoretical capacity (3860 mA h/g) among possible anode materials [11]. In a typical LIB, a stable solid electrolyte interface (SEI) layer is spontaneously formed between the graphite anode and organic electrolyte. A stable SEI can prevent the reduction of electrolytes and facilitate the flux and de-solvation of lithium ions, therefore greatly increasing the cycling stability of the anode [12]. Although a lithium metal anode shares the same principle of redox chemistries as a graphite anode, a SEI formed over a lithium metal anode is intrinsically unstable [13]. The compositional inhomogeneity of such SEI layer leads to poor transport of lithium ions, repeated exposure of fresh lithium and consequent electrolyte depletion and formation of detrimental lithium dendrites [14,15]. Therefore, it is critical to create a conformal SEI layer that can regulate the lithium ion flux on the lithium metal anode surface while being mechanically robust and ionically conductive.

Previously, two types of artificial SEI for lithium metal have been extensively explored – polymer and inorganic coatings [14,16]. Polymer coatings could be easily formed by solution casting or formed in situ, exhibiting a certain extent of flexibility/flowability [17]. However,

* Corresponding author. Department of Materials Science and Engineering, Carnegie Mellon University, 5000 Forbes Ave, Pittsburgh, PA, 15213, USA.
** Corresponding author.
E-mail addresses: sipeili@mit.edu (S. Li), tongliu2@andrew.cmu.edu (T. Liu), jiajunyan@lbl.gov (J. Yan), jflum@andrew.cmu.edu (J. Flum), hw2@andrew.cmu.edu (H. Wang), florandi@andrew.cmu.edu (F. Lorandi), zongyuw@andrew.cmu.edu (Z. Wang), liyef@andrew.cmu.edu (L. Fu), leimingh@andrew.cmu.edu (L. Hu), yuqizhao@andrew.cmu.edu (Y. Zhao), ryuan@andrew.cmu.edu (R. Yuan), mingkans@andrew.cmu.edu (M. Sun), whitacre@andrew.cmu.edu (J.F. Whitacre), matyjaszewski@cmu.edu (K. Matyjaszewski).
[1] These authors contributed equally to this work.

https://doi.org/10.1016/j.nanoen.2020.105046
Received 30 April 2020; Received in revised form 22 May 2020; Accepted 1 June 2020
Available online 3 July 2020

typical polymer coatings have low ionic conductivity ($<10^{-5}$ S/cm at room temperature) and poor mechanical strength, especially when swollen by organic electrolyte. Moreover, due to the low transference number of most polymer materials [18,19], they are inefficient at regulating the flux of lithium ions at the anode/electrolyte interface. Conversely, inorganic coatings, such as SiO_2, Al_2O_3, ZnO, etc., have been proposed as an alternative, because of their high shear modulus, functionality, and lithiophilicity [20–24]. Nevertheless, vague and inconsistent coating preparation procedures limit the applicability of inorganic SEI. Moreover, typical brittle inorganic layers cannot withstand the anode volume fluctuation during lithium plating/stripping [20]. Therefore, it is compelling to fabricate an inorganic/polymer hybrid SEI that combines advantages of both types of artificial SEI (i.e. facile preparation, high flexibility, ductility, transference number, and ionic conductivity) and overcomes their respective weaknesses.

In this work, we created inorganic/polymer hybrid hairy nanoparticles by covalently grafting polyacrylonitrile (PAN) from oxygen vacancy (V_o)-rich yttria-stabilized zirconia nanoparticles (YSZ NPs) via surface-initiated atom transfer radical polymerization (SI-ATRP). The obtained YSZ-*g*-PAN hybrids (Fig. 1a) perform as effective artificial SEI. PAN was chosen due to its wide electrochemical stability window, high ionic conductivity, and good membrane forming ability [25]. PAN has low swellability in typical liquid electrolytes. YSZ is an oxide-ion conductor with good conductivity and chemical/mechanical stability, frequently used in solid oxide fuel cells. By doping ZrO_2 with Y_2O_3, Zr^{4+} ions are partially replaced by Y^{3+} ions in the crystal lattice, resulting in the generation of positively charged oxygen vacancies V_o [26,27]. When coating Li metal with the hybrid materials, the positive surface charges of YSZ NPs can selectively trap the anions, reducing the ion gradient near the anode, and increasing the lithium transference number and conductivity, while homogenizing the ion flux during lithium plating [28]. Furthermore, compared to non-covalent YSZ/PAN blends, covalently grafted hairy NPs further improve the efficiency of the artificial SEI (Fig. 1b&c), due to the following rational: (a) YSZ-*g*-PAN is better dispersed in organic solvents than non-covalent blends, resulting in higher membrane homogeneity and higher mechanical integrity by avoiding particle aggregation and phase separation; (b) the reduced crystallinity and hindered entanglement of polymer chains provided by the star-like conformation of YSZ-*g*-PAN further increase the ionic conductivity of the artificial SEI; (c) the YSZ-*g*-PAN based artificial SEI promotes more uniform ion transport paths, avoiding uneven lithium deposition typically caused by compositional inhomogeneity. In general, the YSZ NPs contributed to accelerate and uniformly distribute the Li^+ flux, while the grafted PAN polymer chains maintained good structural integrity. Therefore, the SEI layer could enable uniform Li deposition with suppressed dendrite growth and regular morphology [29,30].

2. Results and discussion

2.1. Preparation of YSZ-g-PAN hairy NPs

Key to the creation of inorganic/polymer hairy NPs is the availability of a chemical process that allows for tethering of polymer chains onto inorganic components. This process may involve non-covalent coordination, thus being sensitive to minor differences in surface chemical composition and charge. As a result, it remains a challenge to effectively graft polymers onto inorganic substrates. Alternatively, controlled radical polymerization is a suitable tool for grafting various polymers from the surface of inorganic particles, due to the chain-growth nature and the modifiability of initiating sites [31–34].

Recently, our group reported fatty-acid derived initiators to graft polymers from metals and metal oxides nanoparticles by surface-initiated atom transfer radical polymerization (SI-ATRP) [35–37]. YSZ nanoparticles are a metal oxide, and therefore are suitable for surface-functionalization by these tetherable ATRP initiators due to the abundance of surface charges and hence could be used to polymerize acrylonitrile (AN) by ATRP [37]. However, a typical initiator, 12-(2-bromoisobutyramido)dodecanoic acid (BiBADA), contains a 2-bromoisobutyramide initiating group, which is far less reactive in ATRP than the polyacrylonitrile chain end (PAN-Br) [38]. To overcome this reactivity mismatch, we designed and synthesized a new fatty-acid-derived initiator, 12-(2-bromo-2-phenylacetamido)

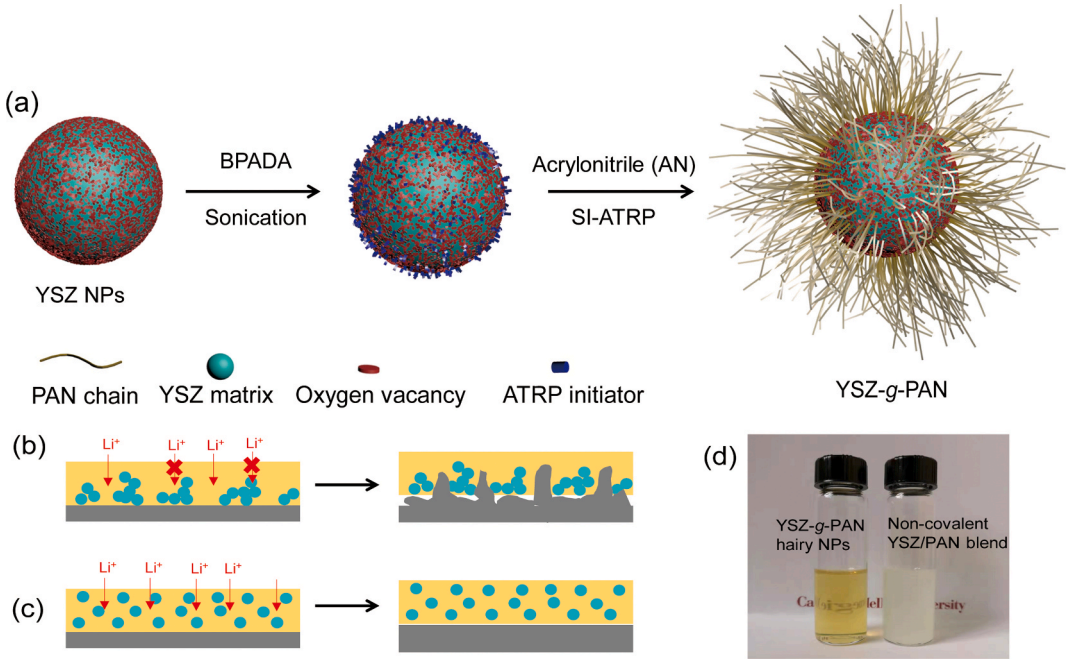

Fig. 1. (a) Synthetic route to YSZ-*g*-PAN hairy nanoparticles. (b) Non-uniform coating prepared from a non-covalent blend of YSZ NPs and PAN/$LiClO_4$ leads to uneven lithium deposition. (c) Uniform hybrid coating using YSZ-*g*-PAN/$LiClO_4$ leads to dendrite-free lithium deposition. (d) Transparent solution (3 wt%) of YSZ-*g*-PAN hairy NPs with 24.6 wt% inorganic content dispersed in DMF (left) and opaque dispersion in DMF of non-covalent blend of YSZ NPs and PAN with identical composition (right).

dodecanoic acid (BPADA), that is more compatible with growing well-defined PAN chains (Scheme S1). 2-Bromo-2-phenylacetic acid (BPAA) was first activated with *N*-hydroxysuccinimide (NHS) to differentiate its reactivity from the carboxylic group of 12-aminolauric acid. This step was followed by the amidation reaction. To immobilize ATRP initiators onto the surface of YSZ NPs, BPADA and YSZ NPs were sonicated together in the presence of triethylamine (TEA). The material obtained upon sonication could not be fully precipitated from tetrahydrofuran (THF), even at a rotational centrifugal force (RCF) of 4000 G, indicating successful anchoring of organic moieties onto the inorganic surface, thus yielding initiator-functionalized YSZ NPs. Thermogravimetric analysis (TGA) and Fourier transform infrared spectroscopy (FTIR) further confirmed the attachment of initiator molecules on YSZ NPs (Figs. S1 and S2). SI-ATRP of AN was performed via initiator for continuous activator regeneration (ICAR) ATRP, using 50–200 ppm of a Cu catalyst [39]. Upon polymerization, the solution was purified by dialysis against dimethylformamide (DMF).

A series of hybrid hairy nanoparticles was prepared with inorganic contents ranging from 7.9 wt% to 71.1 wt% (Table S1). Fig. 1d shows the enhanced solvent dispersibility of YSZ NPs with covalently grafted PAN vs. a non-covalent blend of the same composition. The left picture is a DMF solution of 3 wt% YSZ-*g*-PAN with 24.6 wt% inorganic content after 6 months. The sample formed a transparent solution proving the excellent dispersibility of the grafted system. In comparison, the right picture of Fig. 1d illustrates a just prepared opaque dispersion of a non-covalent blend of a similar weight fraction of YSZ NPs and PAN. The uniform size distribution of covalently grafted hybrid nanoparticles was further confirmed by dynamic light scattering (DLS) analysis, as shown in Fig. 2a. YSZ-*g*-PAN samples with different inorganic content all showed narrow size distribution in DMF. Specifically, samples with inorganic contents of 7.9 wt%, 13.5 wt%, 24.6 wt%, and 71.1 wt%, respectively, had an average size of 377.9 nm, 325.7 nm, 228.7 nm, and 204.6 nm (Table S1). The grafted PAN chains were isolated by etching NPs with HF. Molecular weights (MWs) of the PAN polymers were measured by gel permeation chromatography (GPC). As shown in Fig. 2b and Table S1, samples with inorganic contents of 7.9 wt%, 13.5 wt%, 24.6 wt%, and 71.1 wt% had a M_n of 253,500, 136,300, 79,410, and 18,920, respectively, indicating that the size of the YSZ-*g*-PAN hybrids is correlated to the length of the grafted polymer chains. Transmission electron microscopy (TEM) images of YSZ-*g*-PAN with inorganic contents of 13.5 wt% (Fig. S3), 24.6 wt% (Figs. 2c), and 71.1 wt% (Fig. S4) showed uniformly distributed YSZ NPs with little noticeable aggregations. In comparison, a blend of YSZ NPs (24.6 wt%) and PAN showed high extent of particle aggregation (Fig. S5). These results confirm the advantage of the covalent grafting-from approach that provides uniform NPs distribution in a polymer matrix. The YSZ-*g*-PAN hybrids showed excellent dispersibility also in dimethylsulfoxide (DMSO), which was subsequently used as a solvent for the sample coating due to its stability against Li metal. Noticeably, during the early stage of polymerization, the functionalized nanoparticles exhibited relatively low dispersibility. Thus, to reproducibly prepare samples with good uniformity at high inorganic content remains a challenge, and it will be the focus of our future work.

2.2. Characterizations of artificial SEI

The artificial SEI was prepared by drop casting a DMSO solution containing YSZ-*g*-PAN hairy NPs and $LiClO_4$ onto the surface of fresh lithium chips (Fig. S6). For comparison, a non-covalent blend of YSZ NPs and PAN with $LiClO_4$ was also prepared and drop casted onto Li metal. The thickness of different artificial SEI layers was revealed by cross-sectional scanning electron microscope (SEM). In Fig. S7, artificial layer consisted of YSZ-*g*-PAN/$LiClO_4$ hairy NPs and YSZ NPs/PAN/$LiClO_4$ non-covalent blends both showed thickness ~10 μm, which corresponded to the amount of the casting solution on lithium chip.

Focused ion beam scanning electron microscope (FIB-SEM) was used to study the particle distribution of the artificial SEI (Fig. 3a and Figs. S8–10). Uniform distributions of YSZ NPs were observed for samples prepared from YSZ-*g*-PAN hairy NPs with inorganic content of 13.5 wt% (Fig. S8) and 24.6 wt% (Fig. 3a), indicating the homogeneity of the artificial SEI. In comparison, the coating made of YSZ/PAN non-covalent blend (inorganic content = 24.6 wt%) showed high extent of particle aggregation (Figs. S7 and S9). Interestingly, the artificial SEI prepared from YSZ-*g*-PAN NPs with 71.1 wt% inorganic content showed aggregations and gyroid-phase-like morphology (Fig. S10).

To quantify the mechanical properties, nanoindentation was performed on films made of YSZ-*g*-PAN hairy NPs (inorganic content 24.6 wt%) and $LiClO_4$ and membranes made of the non-covalent blend with the same composition, respectively. Characteristic force-displacement curves for the two samples are presented in Fig. 3b. No pile-up or sink-in were observed, allowing for the standard Oliver and Pharr analysis to be applied to calculate Young's modulus and hardness [40]. The results indicated that the artificial SEI based on YSZ-*g*-PAN hairy NPs showed both higher Young's modulus ($E \sim 7.56$ GPa) and higher hardness ($H \sim 0.34$ GPa) than that of the non-covalent blend ($E \sim 4.65$ GPa and $H \sim 0.22$ GPa) and pure PAN ($E \sim 4.00$ GPa and $H \sim 0.19$ GPa). Such superiority of the mechanical properties should be attributed to the higher uniformity of membranes prepared from YSZ-*g*-PAN hairy NPs.

Electrochemical impedance spectroscopy (EIS) was used to measure the ionic conductivity of membranes. Encouragingly, all YSZ-*g*-PAN/$LiClO_4$ with different inorganic contents showed greatly improved ionic conductivity compared to pure PAN/$LiClO_4$ or non-covalent blend of YSZ/PAN and $LiClO_4$ (Fig. 3c). Samples with inorganic contents of 7.9 wt%, 13.5 wt%, 24.6 wt% and 71.1 wt% showed room-temperature ionic conductivity of 0.33×10^{-4} S/cm, 1.35×10^{-4} S/cm 1.49×10^{-4} S/cm and 0.65×10^{-4} S/cm respectively, which are about two orders of magnitude higher than the ionic conductivity of the non-covalent YSZ/PAN/$LiClO_4$ blend (inorganic content 24.6 wt%). Even

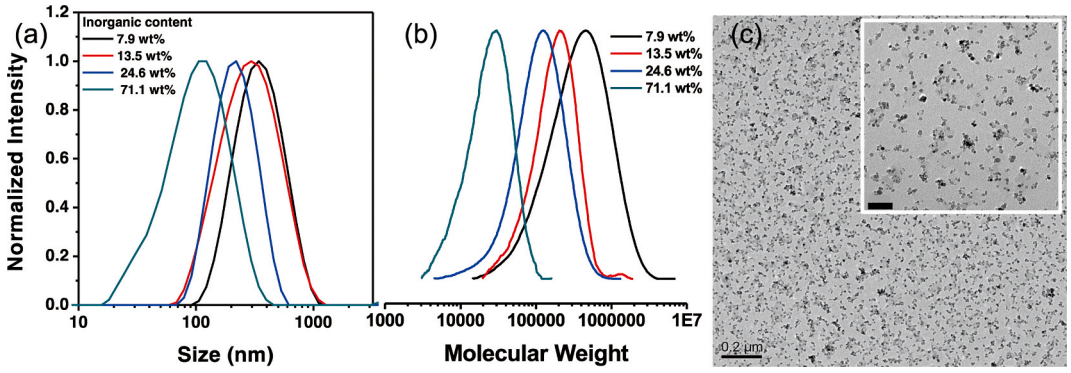

Fig. 2. (a) DLS traces of YSZ-*g*-PAN with different inorganic content. (b) GPC traces of cleaved PAN chains. (c) TEM image of YSZ-*g*-PAN with 24.6 wt% inorganic content (Scale bar = 200 nm), inset: zoomed-in image (Scale bar = 50 nm).

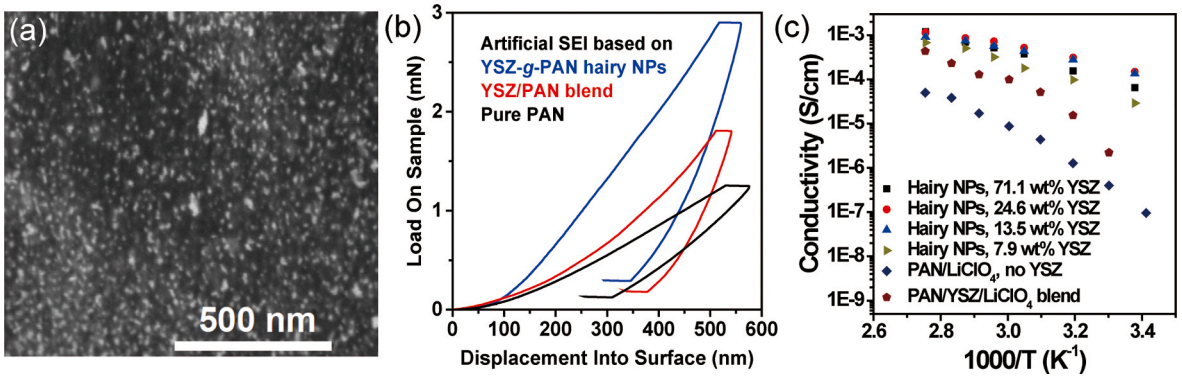

Fig. 3. (a) FIB-SEM image of cross-section of the artificial SEI formed using YSZ-*g*-PAN with inorganic content of 24.6 wt%. (b) Characteristic load–displacement curves of artificial SEI using YSZ-*g*-PAN with inorganic content of 24.6 wt%, artificial SEI using the non-covalent YSZ/PAN blends of the same composition and pure PAN. (c) Arrhenius plots of ionic conductivity of artificial SEI prepared by mixing $LiClO_4$ and YSZ-*g*-PAN hairy NPs of different inorganic content or YSZ/PAN blend (inorganic content 24.6 wt%) or pure PAN.

distribution of YSZ NPs and greater homogeneity are responsible for the enhanced ionic conductivity of the hairy NPs membranes. At 90 °C, the ionic conductivities increased to 6.4×10^{-4} S/cm, 9.16×10^{-4} S/cm, 1.15×10^{-3} S/cm and 1.20×10^{-3} S/cm respectively, suggesting that inorganic content of 24.6 wt% gave the best overall lithium ion transport properties.

2.3. Cycling performance of artificial SEI

Finally, three types of YSZ-*g*-PAN hybrid hairy NPs with inorganic content of 13.5 wt%, 24.6 wt%, and 71.1 wt% were tested as artificial SEI and were compared to artificial SEIs made of pure PAN/$LiClO_4$ and non-covalent blend of YSZ/PAN/$LiClO_4$. To demonstrate the effective dendrite suppression of the artificial SEI, an optical microscope was used to detect the surface roughness of the lithium anode. A home-made visualization cell was designed for the experiment (Fig. S11). Under a current density of 5 mA/cm^2, formation of mossy lithium dendrites on unprotected lithium was observed after less than 2 min (Fig. 4a). In contrast, the surface of lithium anode coated with the YSZ-*g*-PAN/$LiClO_4$ artificial SEI remained smooth for over 10 min, indicating non-existence of dendrite formation (Fig. 4b). To demonstrate the coating benefits on lithium plating/stripping, symmetric cells made of two equivalent lithium anodes with or without protection of artificial SEI were assembled and run at a current density of 3 mA/cm^2 with 1 h for each half step. The cell with unprotected lithium started to polarize immediately and reached about 300 mV overpotential within 200 h before shortage (Fig. 4c). The cell with lithium protected with a non-covalent blend of YSZ NPs/PAN/$LiClO_4$ (24.6 wt%) showed a reduced overpotential, slightly above 100 mV, and longer cycle life, indicating the effectiveness of coating lithium with YSZ NPs added into the polymer matrix. Finally, lithium protected with artificial SEI made from YSZ-*g*-PAN hairy NPs was tested. The artificial SEI with 13.5 wt% inorganic content provided

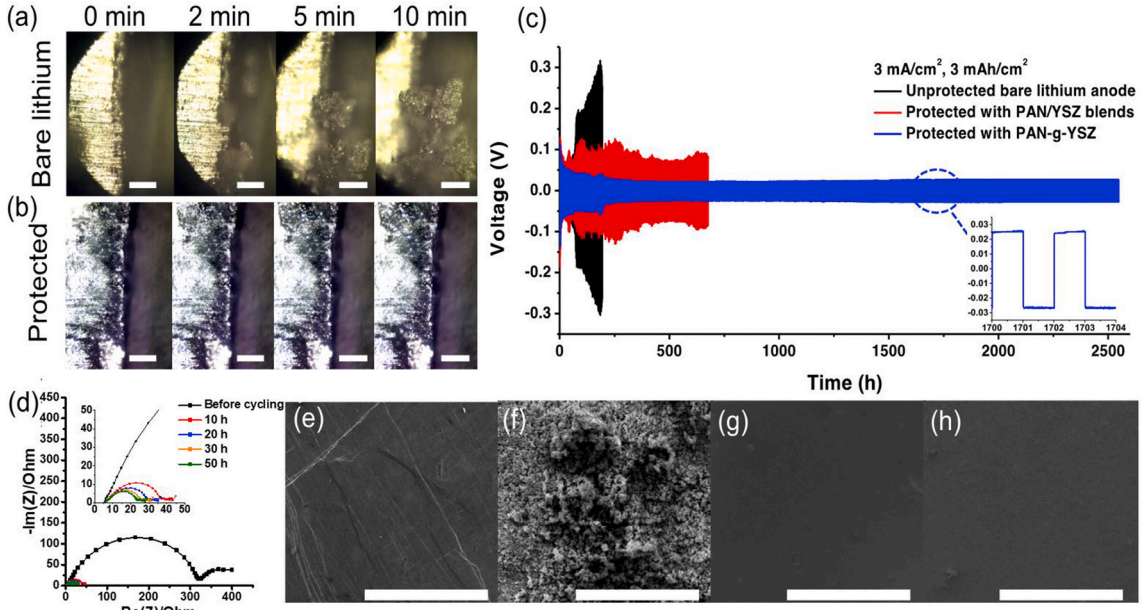

Fig. 4. (a) Optical microscope image of the surface of unprotected lithium during lithium deposition at a current density of 5 mA/cm^2 (scale bar = 100 μm). (b) Optical microscope image of the surface of lithium protected with artificial SEI using YSZ-*g*-PAN hairy NPs with 24.6 wt% inorganic content during lithium deposition at a current density of 5 mA/cm^2 (scale bar = 100 μm). (c) Symmetric cycling of protected lithium using YSZ-*g*-PAN hairy NPs with 24.6 wt% inorganic content (blue), YSZ/PAN non-covalent blend (red) and unprotected lithium anode (black) at a current density of 3 mA/cm^2, 1 h each half step. Inset, detailed voltage profile. (d) Cell resistance measured by EIS during the symmetric cycling of lithium protected with artificial SEI using YSZ-*g*-PAN hairy NPs with 24.6 wt% inorganic content. (e)&(f) SEM images of bare lithium anode before and after 500 h cycling at 3 mA/cm^2. Scale bar = 300 μm. (g)&(h) SEM images of lithium anode protected with artificial SEI using YSZ-*g*-PAN hairy NPs with 24.6 wt% inorganic content before and after 2000 h cycling at 3 mA/cm^2. Scale bar = 300 μm.

an initial overpotential of about 100 mV. As the cycling proceeded, the voltage decreased and stabilized at about 25 mV for over 350 h, then the cell eventually shorted (Fig. S12). With increasing the inorganic content, the symmetric cycling showed even more improved cycling stability. The symmetric cell with electrodes coated with artificial SEI having 71.1 wt% inorganic content lasted for over 2300 h at 3 mA/cm^2. However, the initial voltage showed certain degree of instability after 250–300 h (Fig. S13). This was possibly due to the relatively high brittleness of the membrane with such high inorganic content, as well as its reduced ionic conductivity. Noticeably, higher inorganic content resulted in larger fraction of oxygen vacancies, which could enhance the transference, moreover narrower channels for ion transport could be formed improving the dendrite blocking ability [41,42]. Therefore, even if the sample with 71.1 wt% inorganic content had lower uniformity, it enabled better cycling performance than the sample with 13.5 wt% inorganic content. The electrodes protected with artificial SEI made of YSZ-*g*-PAN NPs with 24.6 wt% inorganic content, which has higher inorganic content than 13.5 wt% as well as high uniformity, showed the best cycling performance, lasting for over 2500 h with overpotential of about 20 mV (Fig. 4c). This cell also achieved the highest Coulombic efficiency of 99.23% (Table S2), which was measured using a well-established approach [43].

The DC resistance of cells made of protected or unprotected lithium was measured by EIS before and after cycling for 50 h. In Fig. 4d, the cell with lithium protected by YSZ-*g*-PAN artificial SEI having 24.6 wt% inorganic content showed resistance of 300 Ohm before cycling, which was reasonable for a typical symmetrical lithium metal cell in liquid electrolyte system, after cycling for 10 h, the activation and consolidation of the artificial SEI reduced the cell resistance to 40 Ohm. As the operation duration extends, the gradual stabilization of the coating layer resulted in the continuous decrease of the cell resistance. (Fig. S15). In comparison, the cell with bare lithium (Fig. S14) exhibited higher and unstable resistance both before and after cycling.

SEM was used to study the surface morphology of electrodes before and after cycling. Fig. 4e and f showed clear formation of lithium dendrites for lithium without protection of the artificial SEI. In comparison, for lithium protected with the artificial SEI, no dendrite formation was observed on the surface (Fig. 4g and h), confirming the efficient protection by YSZ-*g*-PAN artificial SEI.

Fig. S16 shows the cross-sectional and top-view SEM images of coated and bare Li after cycling to reveal their morphology. The symmetric cells were disassembled after cycling for 200 h at 3 mA/cm^2. The Li metal protected with YSZ-*g*-PAN/$LiClO_4$ showed a smooth coating layer and a dense and uniform section of Li metal. In contrast, the Li metal coated with YSZ/PAN/$LiClO_4$ blend showed a less homogeneous but preserved layer and a more porous Li metal. Notably, the unprotected Li displayed a porous structure with moss-like Li dendrites.

Full cell tests were conducted to further evaluate the performance of the artificial SEIs (see SI for detailed description). As shown in Fig. S20, the effect of the artificial SEI was explored in $LiNi_{0.8}Co_{0.15}Al_{0.05}O_2$ (NCA)|Li full cells. It should be noted that NCA cathodes with high commercial grade mass loadings (~28 mg/cm^2) are extracted from commercial 18650 cells and such thick cathode is not designed for optimized rate capability but rather for high energy application. The purpose of using such cathode is to create harsh conditions (amount of Li that move through the SEI layer) to test the practicability of the SEI, as well as to compare the anodes with and without the protection of the artificial SEI. The stability test was conducted at 1C rate between 2.5 V and 4.2 V (Fig. S20a). The cell with Li metal protected by the YSZ-*g*-PAN/$LiClO_4$ artificial SEI (inorganic content 24.6 wt%) exhibited higher capacity retention after 50 cycles than the cell with Li metal coated by YSZ/PAN/$LiClO_4$ non-covalent blend. Moreover, the capacity retention was largely improved compared to unprotected Li. The enhanced stability is likely due to the greater uniformity of the coating which promotes even Li deposition, as observed in symmetric cycling test. The rate capability tests (Fig. S20b) showed that the YSZ-*g*-PAN/$LiClO_4$ artificial SEI enabled higher specific discharge capacity than the YSZ/PAN/$LiClO_4$ non-covalent blend artificial SEI and the unprotected Li at all rates, 1C (140 mA h/g), 2C (90 mA h/g) and 4C (53 mA h/g). The improvement relative to unprotected Li became more evident with increasing the current density. This suggests that the YSZ-*g*-PAN/$LiClO_4$ artificial SEI helps reducing the polarization by promoting uniform current distribution and higher ionic conductivity.

3. Conclusion

We have developed a fatty-acid-based ATRP initiator for grafting PAN from V_o-rich YSZ NPs with high grafting density by SI-ATRP. The as synthesized YSZ-*g*-PAN hairy NPs with different inorganic contents were stably dispersed in organic solvents, without precipitation for several months. The immobilization of PAN chains on the surface of YSZ NPs reduced the polymer crystallinity, therefore increasing the ionic conductivity of the polymer matrix, while improving its mechanical integrity and membrane-forming ability. The positively charged oxygen vacancies of the YSZ NPs further reduced the ion gradient near the anode and increased the conductivity while homogenizing the ion flux during lithium plating. The aforementioned benefits combined with the easiness of solution drop-casting led to the facile creation of hybrid artificial SEIs that enabled dendrite-free lithium plating/stripping with Coulombic efficiency as high as 99.23%. Full cell tests with high mass loadings of commercial grade NCA cathode materials showed that the YSZ-*g*-PAN artificial SEI enabled to achieve higher specific discharge capacities at different rates and improved capacity retention compared to unprotected Li metal and Li coated with a non-covalent blends of YSZ and PAN. The invention of YSZ-*g*-PAN hairy NPs enriches the field of polymer-inorganic hybrid materials and provides new perspectives for the rational design of dendrite-free lithium anodes.

Declaration of competing interest

All authors have reviewed the criteria covering situations where conflict of interest that might exist. All authors report that there are no cases wherein any financial and/or personal relationships with other people or organizations have or could inappropriately influence (bias) the research done in the course of producing this manuscript.

Acknowledgements

Financial support from National Science Foundation (DMR 1501324) and funding from the ARPA-E IONICS program, award number DE-AR0000780, are graciously acknowledged.

Appendix A. Supplementary data

Supplementary data to this article can be found online at https://doi.org/10.1016/j.nanoen.2020.105046.

References

[1] J.B. Goodenough, K.-S. Park, The li-ion rechargeable battery: a perspective, J. Am. Chem. Soc. 135 (2013) 1167–1176, https://doi.org/10.1021/ja3091438.
[2] M. Armand, J.M. Tarascon, Building better batteries, Nature 451 (2008) 652–657, https://doi.org/10.1038/451652a.
[3] P.K. Nayak, L. Yang, W. Brehm, P. Adelhelm, From lithium-ion to sodium-ion batteries: advantages, challenges, and surprises, Angew. Chem. Int. Ed. 57 (2018) 102–120, https://doi.org/10.1002/anie.201703772.
[4] Z.P. Cano, D. Banham, S. Ye, A. Hintennach, J. Lu, M. Fowler, Z. Chen, Batteries and fuel cells for emerging electric vehicle markets, Nat. Energy 3 (2018) 279–289, https://doi.org/10.1038/s41560-018-0108-1.
[5] X. Kang, Electrolytes and interphases in li-ion batteries and beyond, Chem. Rev. 114 (2014) 11503–11618, https://doi.org/10.1021/cr500003w.
[6] S. Li, H. Wang, J. Cuthbert, T. Liu, J.F. Whitacre, K. Matyjaszewski, A semiliquid lithium metal anode, Joule 3 (2019) 1637–1646, https://doi.org/10.1016/j.joule.2019.05.022.

[7] S. Li, H. Wang, W. Wu, F. Lorandi, J.F. Whitacre, K. Matyjaszewski, Solvent-processed metallic lithium microparticles for lithium metal batteries, ACS Appl. Energy Mater. 2 (2019) 1623–1628, https://doi.org/10.1021/acsaem.9b00107.
[8] W.J. Chung, J.J. Griebel, E.T. Kim, H. Yoon, A.G. Simmonds, H.J. Ji, P.T. Dirlam, R. S. Glass, J.J. Wie, N.A. Nguyen, B.W. Guralnick, J. Park, Á. Somogyi, P. Theato, M. E. Mackay, Y.-E. Sung, K. Char, J. Pyun, The use of elemental sulfur as an alternative feedstock for polymeric materials, Nat. Chem. 5 (2013) 518, https://doi.org/10.1038/nchem.1624. https://www.nature.com/articles/nchem.1624#supplementary-information.
[9] L. Li, T.A. Pascal, J.G. Connell, F.Y. Fan, S.M. Meckler, L. Ma, Y.-M. Chiang, D. Prendergast, B.A. Helms, Molecular understanding of polyelectrolyte binders that actively regulate ion transport in sulfur cathodes, Nat. Commun. 8 (2017) 2277, https://doi.org/10.1038/s41467-017-02410-6.
[10] P.G. Bruce, S.A. Freunberger, L.J. Hardwick, J.-M. Tarascon, Li–o2 and li–s batteries with high energy storage, Nat. Mater. 11 (2012) 19–29, https://doi.org/10.1038/nmat3191.
[11] P. Albertus, S. Babinec, S. Litzelman, A. Newman, Status and challenges in enabling the lithium metal electrode for high-energy and low-cost rechargeable batteries, Nat. Energy 3 (2018) 16–21, https://doi.org/10.1038/s41560-017-0047-2.
[12] W. Martin, The solid electrolyte interphase - the most important and the least understood solid electrolyte in rechargeable li batteries, Z. Phys. Chem. 223 (2009) 1395–1406, https://doi.org/10.1524/zpch.2009.6086.
[13] M. Jiang, Y. Xie, H. Xu, J. Jia, Developing high-performance lithium metal anode in liquid electrolytes: challenges and progress, Adv. Mater. (2018) 30, https://doi.org/10.1002/adma.201706375.
[14] M.D. Tikekar, S. Choudhury, Z. Tu, L.A. Archer, Design principles for electrolytes and interfaces for stable lithium-metal batteries, Nat. Energy 1 (2016) 16114, https://doi.org/10.1038/nenergy.2016.114.
[15] X.-B. Cheng, R. Zhang, C.-Z. Zhao, F. Wei, J.-G. Zhang, Q. Zhang, A review of solid electrolyte interphases on lithium metal anode, Adv. Sci. 3 (2016) 1500213, https://doi.org/10.1002/advs.201500213.
[16] D. Lin, P.Y. Yuen, K. Liu, J. Xie, An artificial solid electrolyte interphase with high li-ion conductivity, mechanical strength, and flexibility for stable lithium metal anodes, Adv. Mater. (29) (2017), https://doi.org/10.1002/adma.201605531.
[17] S. Xia, X. Wu, Z. Zhang, Y. Cui, W. Liu, Practical challenges and future perspectives of all-solid-state lithium-metal batteries, Inside Chem. 5 (2019) 753–785, https://doi.org/10.1016/j.chempr.2018.11.013.
[18] S. Li, A.I. Mohamed, V. Pande, H. Wang, J. Cuthbert, X. Pan, H. He, Z. Wang, V. Viswanathan, J.F. Whitacre, K. Matyjaszewski, Single-ion homopolymer electrolytes with high transference number prepared by click chemistry and photoinduced metal-free atom-transfer radical polymerization, ACS Energy Lett. 3 (2018) 20–27, https://doi.org/10.1021/acsenergylett.7b00999.
[19] R. Bouchet, S. Maria, R. Meziane, A. Aboulaich, L. Lienafa, J.-P. Bonnet, T.N. T. Phan, D. Bertin, D. Gigmes, D. Devaux, R. Denoyel, M. Armand, Single-ion bab triblock copolymers as highly efficient electrolytes for lithium-metal batteries, Nat. Mater. 12 (2013) 452–457, https://doi.org/10.1038/nmat3602.
[20] C.-Z. Zhao, Q. Zhang, Constructing conformal interface by semiliquid li metal, Joule 3 (2019) 1575–1577, https://doi.org/10.1016/j.joule.2019.06.019.
[21] R. Xu, X.-B. Cheng, C. Yan, X.-Q. Zhang, Y. Xiao, C.-Z. Zhao, J.-Q. Huang, Q. Zhang, Artificial interphases for highly stable lithium metal anode, Matter 1 (2019) 317–344, https://doi.org/10.1016/j.matt.2019.05.016.
[22] L. Chen, J.G. Connell, A. Nie, Z. Huang, K.R. Zavadil, K.C. Klavetter, Y. Yuan, S. Sharifi-Asl, R. Shahbazian-Yassar, J.A. Libera, A.U. Mane, J.W. Elam, Lithium metal protected by atomic layer deposition metal oxide for high performance anodes, J. Mater. Chem. 5 (2017) 12297–12309, https://doi.org/10.1039/C7TA03116E.
[23] J. Xie, J. Wang, H.R. Lee, K. Yan, Y. Li, F. Shi, W. Huang, A. Pei, G. Chen, R. Subbaraman, J. Christensen, Y. Cui, Engineering stable interfaces for three-dimensional lithium metal anodes, Sci. Adv. 4 (2018), https://doi.org/10.1126/sciadv.aat5168 eaat5168.
[24] B. Zhu, N. Liu, M. McDowell, Y. Jin, Y. Cui, J. Zhu, Interfacial stabilizing effect of zno on si anodes for lithium ion battery, Nano Energy 13 (2015) 620–625, https://doi.org/10.1016/j.nanoen.2015.03.019.
[25] Y.W. Chen-Yang, H.C. Chen, F.J. Lin, C.C. Chen, Polyacrylonitrile electrolytes: 1. A novel high-conductivity composite polymer electrolyte based on pan, liclo4 and α-al2o3, Solid State Ionics 150 (2002) 327–335, https://doi.org/10.1016/S0167-2738(02)00457-5.
[26] B. Feng, N.R. Lugg, A. Kumamoto, Y. Ikuhara, N. Shibata, Direct observation of oxygen vacancy distribution across yttria-stabilized zirconia grain boundaries, ACS Nano 11 (2017) 11376–11382, https://doi.org/10.1021/acsnano.7b05943.
[27] A. Kushima, B. Yildiz, Oxygen ion diffusivity in strained yttria stabilized zirconia: where is the fastest strain? J. Mater. Chem. 20 (2010) 4809–4819, https://doi.org/10.1039/C000259C.
[28] W. Liu, D. Lin, J. Sun, G. Zhou, Y. Cui, Improved lithium ionic conductivity in composite polymer electrolytes with oxide-ion conducting nanowires, ACS Nano 10 (2016) 11407–11413, https://doi.org/10.1021/acsnano.6b06797.
[29] C. Wang, A. Wang, L. Ren, X. Guan, D. Wang, A. Dong, C. Zhang, G. Li, J. Luo, Controlling li ion flux through materials innovation for dendrite-free lithium metal anodes, Adv. Funct. Mater. 29 (2019) 1905940, https://doi.org/10.1002/adfm.201905940.
[30] X. Sun, X. Zhang, Q. Ma, X. Guan, W. Wang, J. Luo, Revisiting the electroplating process for lithium-metal anodes for lithium-metal batteries, Angew. Chem. Int. Ed. 59 (2020) 6665–6674, https://doi.org/10.1002/anie.201912217.
[31] S. Li, K. Jiang, J. Wang, C. Zuo, Y.H. Jo, D. He, X. Xie, Z. Xue, Molecular brush with dense peg side chains: design of a well-defined polymer electrolyte for lithium-ion batteries, Macromolecules 52 (2019) 7234–7243, https://doi.org/10.1021/acs.macromol.9b01641.
[32] C. Li, S. Liu, C. Shi, G. Liang, Z. Lu, R. Fu, D. Wu, Two-dimensional molecular brush-functionalized porous bilayer composite separators toward ultrastable high-current density lithium metal anodes, Nat. Commun. 10 (2019) 1363, https://doi.org/10.1038/s41467-019-09211-z.
[33] L. Porcarelli, A.S. Shaplov, M. Salsamendi, J.R. Nair, Y.S. Vygodskii, D. Mecerreyes, C. Gerbaldi, Single-ion block copoly(ionic liquid)s as electrolytes for all-solid state lithium batteries, ACS Appl. Mater. Interfaces 8 (2016) 10350–10359, https://doi.org/10.1021/acsami.6b01973.
[34] J. Yan, M.R. Bockstaller, K. Matyjaszewski, Brush-modified materials: control of molecular architecture, assembly behavior, properties and applications, Prog. Polym. Sci. (2019) 101180, https://doi.org/10.1016/j.progpolymsci.2019.101180.
[35] J. Yan, S. Li, F. Cartieri, Z. Wang, T.K. Hitchens, J. Leonardo, S.E. Averick, K. Matyjaszewski, Iron oxide nanoparticles with grafted polymeric analogue of dimethyl sulfoxide as potential magnetic resonance imaging contrast agents, ACS Appl. Mater. Interfaces 10 (2018) 21901–21908, https://doi.org/10.1021/acsami.8b06416.
[36] J. Yan, M.H. Malakooti, Z. Lu, Z. Wang, N. Kazem, C. Pan, M.R. Bockstaller, C. Majidi, K. Matyjaszewski, Solution processable liquid metal nanodroplets by surface-initiated atom transfer radical polymerization, Nat. Nanotechnol. 14 (2019) 684–690, https://doi.org/10.1038/s41565-019-0454-6.
[37] J. Yan, X. Pan, Z. Wang, Z. Lu, Y. Wang, L. Liu, J. Zhang, C. Ho, M.R. Bockstaller, K. Matyjaszewski, A fatty acid-inspired tetherable initiator for surface-initiated atom transfer radical polymerization, Chem. Mater. 29 (2017) 4963–4969, https://doi.org/10.1021/acs.chemmater.7b01338.
[38] W. Tang, K. Matyjaszewski, Effects of initiator structure on activation rate constants in atrp, Macromolecules 40 (2007) 1858–1863, https://doi.org/10.1021/ma062897b.
[39] K. Matyjaszewski, W. Jakubowski, K. Min, W. Tang, J. Huang, W.A. Braunecker, N. V. Tsarevsky, Diminishing catalyst concentration in atom transfer radical polymerization with reducing agents, Proc. Natl. Acad. Sci. Unit. States Am. 103 (2006) 15309, https://doi.org/10.1073/pnas.0602675103.
[40] W.C. Oliver, G.M. Pharr, Measurement of hardness and elastic modulus by instrumented indentation: advances in understanding and refinements to methodology, J. Mater. Res. 19 (2004) 3–20, https://doi.org/10.1557/jmr.2004.19.1.3.
[41] L. Ma, C. Fu, L. Li, K.S. Mayilvahanan, T. Watkins, B.R. Perdue, K.R. Zavadil, B. A. Helms, Nanoporous polymer films with a high cation transference number stabilize lithium metal anodes in light-weight batteries for electrified transportation, Nano Lett. 19 (2019) 1387–1394, https://doi.org/10.1021/acs.nanolett.8b05101.
[42] S. Choudhury, D. Vu, A. Warren, M.D. Tikekar, Z. Tu, L.A. Archer, Confining electrodeposition of metals in structured electrolytes, Proc. Natl. Acad. Sci. Unit. States Am. 115 (2018) 6620, https://doi.org/10.1073/pnas.1803385115.
[43] K.-H. Chen, A.J. Sanchez, E. Kazyak, A.L. Davis, N.P. Dasgupta, Lithium metal anodes: synergistic effect of 3d current collectors and ald surface modification for high coulombic efficiency lithium metal anodes (adv. Energy mater. 4/2019), Adv. Energy Mater. 9 (2019) 1970010, https://doi.org/10.1002/aenm.201970010.

Sipei Li received his Ph.D. in 2019 from Carnegie Mellon University under the supervision of Prof. Krzysztof Matyjaszewski. He then joined Research Lab of Electronics at Massachusetts Institute of Technology as a postdoctoral associate, under the supervision of Prof. Yang Shao-Horn and Prof. Jeremiah Johnson. His research interests include polymer chemistry, solid electrolyte and lithium based rechargeable batteries.

Tong Liu is currently a second-year Ph.D. candidate at Department of Chemistry, Carnegie Mellon University under the supervision of Prof. Krzysztof Matyjaszewski. Her research interests include polymer hybrids, solid electrolyte and lithium metal batteries.

Jiajun Yan received his Ph.D. in 2018 from Carnegie Mellon University under the supervision of Prof. Krzysztof Matyjaszewski. He is currently a postdoctoral scholar in Brett Helms group at Lawrence Berkeley National Laboratory. His research interests include interfacial sciences and polymers with complex architectures.

Jacob Flum received his Master's degree in 2018 from Department of Chemistry, Carnegie Mellon University under the supervision of Prof. Krzysztof Matyjaszewski. His research interest includes synthesis and characterization of self-healing polymers and lithium metal batteries.

Han Wang received his Ph.D. in 2020 from Department of Materials Science and Engineering, Carnegie Mellon University under the supervision of Prof. Jay Whitacre. His research interests include recycling of battery materials and lithium metal batteries.

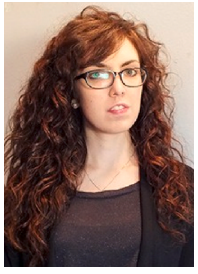

Francesca Lorandi received her Ph.D. in 2018 from University of Padova (Italy), under the supervision of Prof. A. Gennaro. She then joined the Matyjaszewski Polymer Group at Carnegie Mellon University. Her research interests include mechanistic investigations of reversible deactivation radical polymerizations, atom transfer radical polymerization in dispersed media, and development of polymer-based materials for energy storage devices.

Zongyu Wang received his Ph.D. in 2019 from Carnegie Mellon University under the supervision of Prof. Krzysztof Matyjaszewski. He then joined Oak Ridge National Lab as a postdoctoral associate. His research interests include synthesis of polymer at interface and polymer/inorganic hybrids and applications.

Liye Fu received his Ph.D. in 2020 from Department of Chemistry, Carnegie Mellon University under the supervision of Prof. Krzysztof Matyjaszewski. His research interests include synthesis of bio-functional polymers and protein-polymer conjugates.

Leiming Hu received his Ph.D. in 2020 from Department of Mechanical Engineering, Carnegie Mellon University under the supervision of Prof. Shawn Litster. His work focuses on fuel cell durability in extreme temperatures, and developing an understanding of catalyst utilization from a proton transport mechanism perspective.

Yuqi Zhao is a Master's degree candidate at Department of Materials Science and Engineering under the supervision of Prof. Michael Bockstaller. His work focus on structure-property relationship of particle brush materials.

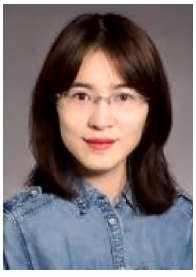

Rui Yuan received her Ph.D. in 2020 from Department of Chemistry, Carnegie Mellon University under the supervision of Prof. Krzysztof Matyjaszewski. Her research interests include carbon-based functional materials and their applications.

Mingkang Sun is currently a third-year Ph.D. candidate at Department of Chemistry, Carnegie Mellon University under the supervision of Prof. Krzysztof Matyjaszewski. His research interests include carbon-based functional materials and their applications.

Jay F. Whitacre is Trustee Professor in Energy and Director of Wilton E. Scott Institute for Energy Innovation. He started his career at the California Institute of Technology/Jet Propulsion Laboratory. Since joining Carnegie Mellon University in 2007, he has focused on the synergistic fields of energy storage and energy system technoeconomic assessment. He has developed a novel battery chemistry/design that is manufactured and sold by Aquion Energy, a company he founded in 2008.

Krzysztof Matyjaszewski is J.C. Warner University Professor of Natural Sciences at Carnegie Mellon University. His current group at CMU includes 17 graduate students and six post-doctoral fellows. In 1994, he discovered Cu-mediated atom transfer radical polymerization, which was commercialized in 2004 in the United States, Japan, and Europe. His research is focused on synthesis of well-defined macromolecules and hybrid materials via living and controlled polymerizations using radical and ionic mechanisms to prepare advanced materials for optoelectronic, biomedical, environmental, and energy-related applications.